

# Expected Complexity of Routing in $\Theta_6$ and Half- $\Theta_6$ Graphs\*

Prosenjit Bose,<sup>†</sup>

Jean-Lou De Carufel,<sup>‡</sup>

Olivier Devillers,<sup>§</sup>

## Abstract

We study online routing algorithms on the  $\Theta_6$ -graph and the half- $\Theta_6$ -graph (which is equivalent to a variant of the Delaunay triangulation). Given a source vertex  $s$  and a target vertex  $t$  in the  $\Theta_6$ -graph (resp. half- $\Theta_6$ -graph), there exists a deterministic online routing algorithm that finds a path from  $s$  to  $t$  whose length is at most  $2\|st\|$  (resp.  $2.89\|st\|$ ) which is optimal in the worst case [Bose *et al.*, SIAM J. on Computing, 44(6)]. We propose alternative, slightly simpler routing algorithms that are optimal in the worst case and for which we provide an analysis of the average routing ratio for the  $\Theta_6$ -graph and half- $\Theta_6$ -graph defined on a Poisson point process.

For the  $\Theta_6$ -graph, our online routing algorithm has an expected routing ratio of 1.161 (when  $s$  and  $t$  are random) and a maximum expected routing ratio of 1.22 (maximum for fixed  $s$  and  $t$  where all other points are random), much better than the worst-case routing ratio of 2. For the half- $\Theta_6$ -graph, our memoryless online routing algorithm has an expected routing ratio of 1.43 and a maximum expected routing ratio of 1.58. Our online routing algorithm that uses a constant amount of additional memory has an expected routing ratio of 1.34 and a maximum expected routing ratio of 1.40. The additional memory is only used to remember the coordinates of the starting point of the route. Both of these algorithms have an expected routing ratio that is much better than their worst-case routing ratio of 2.89.

## 1 Introduction

A weighted geometric graph  $G = (P, E)$  is a graph whose vertex set is a set  $P$  of  $n$  points in the plane, and whose edge set is a set of line segments joining pairs of points in  $P$ , with each edge weighted by the Euclidean distance between its endpoints. A graph  $G$  is a geometric  $\delta$ -spanner of the complete geometric graph provided that for every pair of points  $(s, t) \in P^2$  the shortest path from  $s$  to  $t$  in  $G$  has weight at most  $\delta \geq 1$  times  $\|st\|$ , where  $\delta$  is the *spanning ratio* or *stretch factor* and  $\|st\|$  is the Euclidean distance from  $s$  to  $t$ . The spanning properties of various geometric graphs have been studied extensively in the literature (see [9, 15] for a comprehensive overview of the topic).

A routing algorithm for a geometric graph takes as input a pair of vertices  $(s, t)$  and finds a path from  $s$  to  $t$  in the graph. When full knowledge of the graph is available to the algorithm, numerous routing algorithms exist in the literature for finding paths in these graphs such as Breadth-First Search, Depth-First Search or Dijkstra's algorithm [11–14]. The problem offers different challenges in the *online* setting. By the online setting, we mean that initially, the routing algorithm has limited knowledge of the graph and needs to simultaneously explore the graph while trying to find a path from  $s$  to  $t$ . Without knowledge of the whole graph, a routing algorithm, in general, cannot identify a short path. In certain cases, depending on the information available to the routing algorithm and limitations placed on the algorithm such as how much memory it has, it may not even find a path but may end up cycling without ever reaching its destination [4]. A formal definition of our routing model is given in Section 1.3.

A graph  $G$  being a spanner of the complete graph simply implies the existence of a short path in  $G$  between every pair of vertices. The goal of a competitive online routing algorithm is to find a short path

\*This work has been supported by INRIA Associated team TRIP, by grant ANR-17-CE40-0017 of the French National Research Agency (ANR project ASPAG) and by NSERC.

<sup>†</sup>Carleton University, Ottawa, Canada. [jit@scs.carleton.ca](mailto:jit@scs.carleton.ca)

<sup>‡</sup>University of Ottawa, Ottawa, Canada. [jdecaruf@uottawa.ca](mailto:jdecaruf@uottawa.ca)

<sup>§</sup>Université de Lorraine, CNRS, Inria, LORIA, F-54000 Nancy, France. [olivier.devillers@inria.fr](mailto:olivier.devillers@inria.fr).

when one exists. A routing algorithm is  $\rho$ -competitive if for any two points  $s$  and  $t$ , the length of the path in  $G$  followed by the routing algorithm is not more than  $\rho$  times  $\|st\|$ , where  $\rho$  refers to the *routing ratio* [7]. There is an intimate connection between the spanning and routing ratio. The routing ratio can be viewed as the spanning ratio of the path found by the routing algorithm, thus the routing ratio is an upper bound on the spanning ratio.

Both the spanning ratio and the routing ratio are fragile measures. For example,  $G$  can be the complete graph that is missing only one edge but can still have an unbounded spanning and routing ratio. As such, studying the spanning and routing ratio in the expected sense is a more robust measure. One of the key difficulties in analyzing these ratios in the probabilistic sense is that often there is a lot of dependence in the process used by a routing algorithm to select which edge to follow. To overcome these barriers, we need to define simple routing strategies with good worst-case behaviour that can also be analyzed in the expected sense.

## 1.1 Contribution

This paper has two main contributions. The first contribution consists of the design of two new algorithms for routing in the half- $\Theta_6$ -graph (also known as the *TD*-Delaunay triangulation [2]) in the so called *negative-routing* case, which is challenging since at each step, the routing algorithm must select among many possible edges to follow, some of which lead you astray. Our new routing algorithms come in two flavors: one is memoryless and the other uses a constant amount of memory. These new negative-routing algorithms have a worst-case optimal routing ratio but are simpler and more amenable to probabilistic analysis than the known optimal routing algorithm [7]. We also provide a new point of view on routing [7] in the half- $\Theta_6$ -graph in the *positive-routing* case, which in some sense is identical to the optimal routing algorithm on the  $\Theta_6$ -graph. This new point of view allows us to complete the probabilistic analysis both on the half- $\Theta_6$ -graph and on the  $\Theta_6$ -graph.

The second contribution is the analysis of the two new negative-routing algorithms and of the positive-routing algorithm in a random setting, namely when the vertex set of the  $\Theta_6$ -graph and half- $\Theta_6$ -graph is a point set that comes from an infinite Poisson point process  $X$  of intensity  $\lambda$ . The analysis is asymptotic with  $\lambda$  going to infinity, and gives the expected length of the shortest path between two fixed points  $s$  and  $t$  at distance one. Our results depend on the position of  $t$  with respect to  $s$ . We express our results both by taking the worst position for  $t$  and by averaging over all possible positions for  $t$ .

The routing ratio for our memoryless negative-routing algorithm in the half- $\Theta_6$ -graph is 2.89 in the worst case which is optimal, 1.58 in the expected case for the worst position for  $t$ , and 1.43 in the expected case when averaging over all possible positions for  $t$ . For our constant memory negative-routing algorithm, we obtain a routing ratio of 2.89 in the worst case, 1.40 expected for the worst position for  $t$ , and 1.34 averaging on all possible positions for  $t$ . For the routing ratio of the positive-routing algorithm on the half- $\Theta_6$ -graph, we obtain 2 in the worst case which is optimal, 1.22 expected for the worst position of  $t$ , and 1.16 averaging on all possible positions for  $t$ . Our results on routing in the  $\Theta_6$ -graph are identical to the positive-routing strategy since the  $\Theta_6$ -graph is the union of two half- $\Theta_6$ -graphs and one can locally differentiate the edges between the two spanning subgraphs. Therefore, this algorithm for  $\Theta_6$ -routing is memoryless.

Formal definitions of the online routing model and the different graphs on which we route are outlined in the following subsections.

## 1.2 The Poisson Point Process

A Poisson point process  $X$  of intensity  $\lambda$  in the plane is an infinite set of points satisfying the following properties: the expected number of points of  $X$  in a domain  $A$  is  $\lambda \cdot \text{Area}(A)$  and the number of points of  $X$  in two disjoint domains are independent. The number of points in  $A$  follows a Poisson's law:

$$\mathbb{P}[|X \cap A| = k] = \frac{\lambda^k \text{Area}(A)^k}{k!} e^{-\lambda \text{Area}(A)}$$

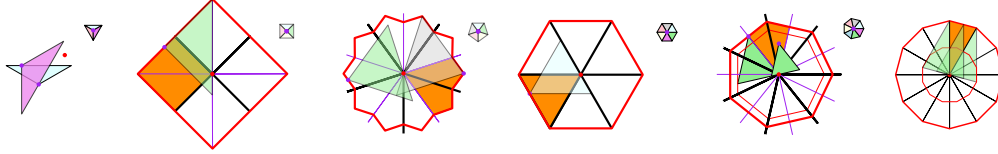


Figure 1: Routing in the  $\Theta_k$ -graph for  $k \in \{3, 4, 5, 6, 7, 8\}$  (from left to right).  $\Theta_3$ -routing to the red point loop between the two purple points.  $\Theta_k$ -routing ( $k \in \{4, 5, 6\}$ ) from the red polygon to the red point goes strictly inside the polygon, thus decrease the polygonal distance to the target and prove that routing will terminate on a finite set of points. For  $k \in \{7, 8, \dots\}$ , one step from the boundary of the red polygon allows to quantify the decrease in polygonal distance to the target and prove that the routing ratio is bounded.

### 1.3 The Online Routing Model

In its weakest form, an online local geometric routing algorithm on a graph  $G = (P, E)$  can be expressed as a *routing function*  $f : P \times P \times \mathcal{P}(P) \rightarrow P$ , where  $\mathcal{P}(\cdot)$  denotes the power set, with parameters  $f(u, t, N(u))$  such that  $u \in P$  is the vertex for which a forwarding decision is being made (i.e., the node currently holding the message),  $t \in P$  is the destination vertex (target), and  $N(u) \subseteq P$  is the set of neighbours of  $u$  in  $G$ . Upon receiving a message destined for  $t$ , node  $u$  forwards the message to its neighbour  $z = f(u, t, N(u)) \in N(u)$ . This routing strategy is referred to as *memoryless* routing. If the routing algorithm uses constant additional memory to store some information  $i \in \mathcal{I}$ , then this information is taken into consideration when computing which neighbour to forward the message to. The function then becomes  $f : P \times P \times \mathcal{P}(P) \times \mathcal{I} \rightarrow P$ . Such a routing strategy is referred to as *constant-memory routing*. In the remainder of the article, we use the additional memory to store the vertex coordinates of the source of the message.

### 1.4 $\Theta_k$ -routing

For any  $k$  the  $\Theta_k$ -graph is defined as follows. For each point  $p \in P$ , consider a set of rays originating from  $p$  with the angle between consecutive rays being  $2\pi/k$ . Each consecutive pair of rays defines a cone. Orient the cones such that there is one cone, labeled  $C_0^p$ , whose bisector is a vertical ray through  $p$  pointing upwards. Label the cones in counterclockwise order:  $C_0^p, \dots, C_{k-1}^p$ . Given two vertices  $p$  and  $q$  define the *canonical triangle*  $T_{pq}$  to be the triangle bounded by the sides of the cone of  $p$  that contains  $q$  and the line through  $q$  perpendicular to the bisector of that cone. An edge in  $\Theta_k$  exists between two vertices  $p$  and  $q$  if  $q$  is in some cone  $C_i^p$ , and for all points  $w \in C_i^p$ ,  $\|pq'\| \leq \|pw'\|$ , where  $p'$  and  $w'$  denote the orthogonal projection of  $p$  and  $w$  onto the bisector of cone  $C_i^p$ . In other words,  $T_{pq}$  contains no points of the point set  $P$ . We say that  $T_{pq}$  is *empty*. The half- $\Theta_k$ -graph is defined similarly for even  $k$  but only half the cones are considered for edge inclusion. Thus, an edge exists between two vertices  $p$  and  $q$  of the half- $\Theta_k$ -graph provided that  $q$  is in some cone  $C_i^p$  where  $i$  is even, and  $T_{pq}$  is empty. The *even cones* refer to the cones with even index and the *odd cones* refer to the ones with odd index. In fact, the  $\Theta_k$ -graph is the union of the half- $\Theta_k$ -graph defined by the even cones and the half- $\Theta_k$ -graph defined by the odd cones.

The structure of the  $\Theta_k$ -graph naturally gives rise to a simple routing algorithm known as  $\Theta_k$ -routing. Let  $t$  be the destination vertex. The  $\Theta_k$ -routing algorithm invoked at an arbitrary vertex  $v$  consists of following the edge adjacent to  $v$  in the cone of  $v$  that contains  $t$ . This process is repeated until the destination  $t$  is reached.

It is known that  $\Theta_k$ -routing terminates with routing ratio  $\rho = 1 + f(k)$  where  $f(k) \in o(1)$  for all  $\Theta_k$ -graphs with  $k \geq 7$  [6, 16]. There is a gap between the best known upper bound on the spanning ratio and  $\rho$  (see [6] for a survey of the best known bounds both on the spanning ratio and  $\rho$ ). For  $k = 2$ , the graph is just the  $y$ -monotone chain of vertices ordered vertically. In this case,  $\Theta_2$ -routing works but the routing ratio is unbounded. For  $k = 3$ , the graph is connected but  $\Theta_3$ -routing may loop as on the example of Figure 1-left [1]. For  $k \in \{4, 5, 6\}$ ,  $\Theta_k$ -routing always finds a path but its length may be unbounded (see Figures 1 and 2). Alternative routing algorithms dedicated specifically for  $\Theta_4$ ,  $\Theta_5$ , and  $\Theta_6$  graphs have been designed proving

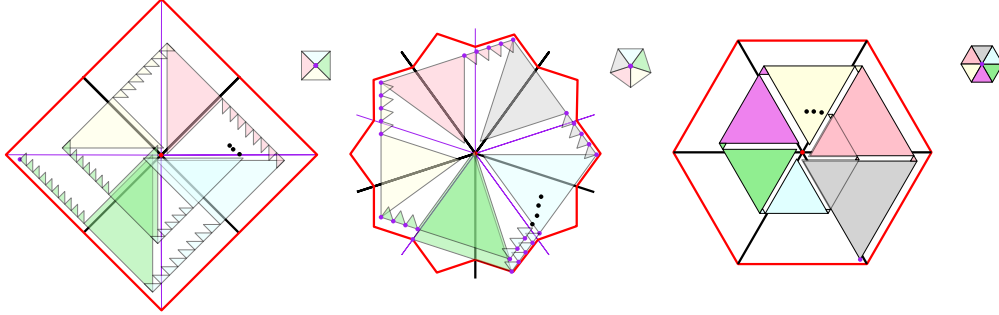


Figure 2: Routing ratio in the  $\Theta_k$ -graph is unbounded for  $k \in \{4, 5, 6\}$

that they have constant routing ratio respectively smaller than 17 [5],  $\sqrt{50 + 22\sqrt{5}} < 10$  [8], and 2 [2, 7]. Bonichon and Marckert [3] analyze the expected length of the  $\Theta_k$ -routing algorithm when the  $\Theta_k$ -graph is defined on a Poisson point process with intensity  $\lambda$  tending to infinity. Their results are much more complete since they address all  $k$  and variants of  $\Theta_k$ -graphs such as Yao-graphs or continuous  $\Theta_k$ -graphs. But these results are limited to the standard  $\Theta_k$ -routing algorithm while we will address different routing algorithms in the sequel.

### 1.5 The $\Theta_6$ -graph and Half- $\Theta_6$ -graph

In the special case  $k = 6$ , the  $\Theta_6$ -graph has some interesting properties. The six rays that define the cones around a point  $p$  make an angle of  $0, \frac{\pi}{3}, \frac{2\pi}{3}, \pi, \frac{4\pi}{3},$  and  $\frac{5\pi}{3}$  with the horizontal axis. The triangles  $T_{pq}$  when  $q$  is in an even (resp. odd) cone  $C_i^p$  are all homothets. This is the key property that is not shared with any other  $\Theta$ -graphs. For other values of  $k$  cones are homothets only when the value of  $i$  is fixed. For  $k = 6$  only the parity of  $i$  matters. Using this property, Bonichon *et al.* [2] noted that the half- $\Theta_6$ -graph is equivalent to the *TD*-Delaunay triangulation. The *TD*-Delaunay triangulation is a variant of the standard Delaunay triangulation where the empty disk property is replaced with an empty homothet of an equilateral triangle (*TD* is an abbreviation for triangular distance).

### 1.6 $\Theta_6$ -routing

As mentioned in Section 1.4,  $\Theta_6$ -routing always terminates but may have an unbounded routing-ratio (see Figures 1 and 2). The analysis by Bonichon and Marckert [3] on  $\Theta_k$ -routing for  $k = 6$  bounds the expected cost of the  $\Theta_6$ -routing algorithm when the point set is defined on a Poisson point process with intensity  $\lambda$  tending to infinity. As noted in Remark 10, our techniques establish the same probabilistic bounds. However the worst case routing ration of the  $\Theta_6$ -routing algorithm is unbounded, see Figure 2. We focus on the probabilistic analysis of routing algorithms that are optimal in the worst-case.

Chew [10] showed that the *TD*-Delaunay triangulation (equivalently the half- $\Theta_6$ -graph) is a 2-spanner. His proof is constructive, however, it does not provide an online routing algorithm that successfully routes between every ordered pair of vertices. Without loss of generality, label the cones of the half- $\Theta_6$ -graph such that the *TD*-Delaunay triangulation is equivalent to the even half- $\Theta_6$ -graph. In this case, positive-routing refers to routing from  $s$  to  $t$  when  $T_{st}$  is even and negative-routing refers to routing from  $s$  to  $t$  when  $T_{st}$  is odd. Chew's algorithm is a positive-routing algorithm and constructs a path from  $s$  to  $t$  with a routing ratio of 2 when  $T_{st}$  is even. Since for every pair of points  $s$  and  $t$ , either  $T_{st}$  is even or  $T_{ts}$  is even, Chew's algorithm proves that the *TD*-Delaunay triangulation is a geometric 2-spanner. However, when  $T_{st}$  is odd, Chew's routing algorithm fails.

Bose *et al.* [7] addressed the negative-routing case providing an algorithm with routing ratio  $\frac{5}{\sqrt{3}} \simeq 2.89$ . Surprisingly, this ratio is optimal for any constant-memory online routing algorithm [7]. This algorithm and

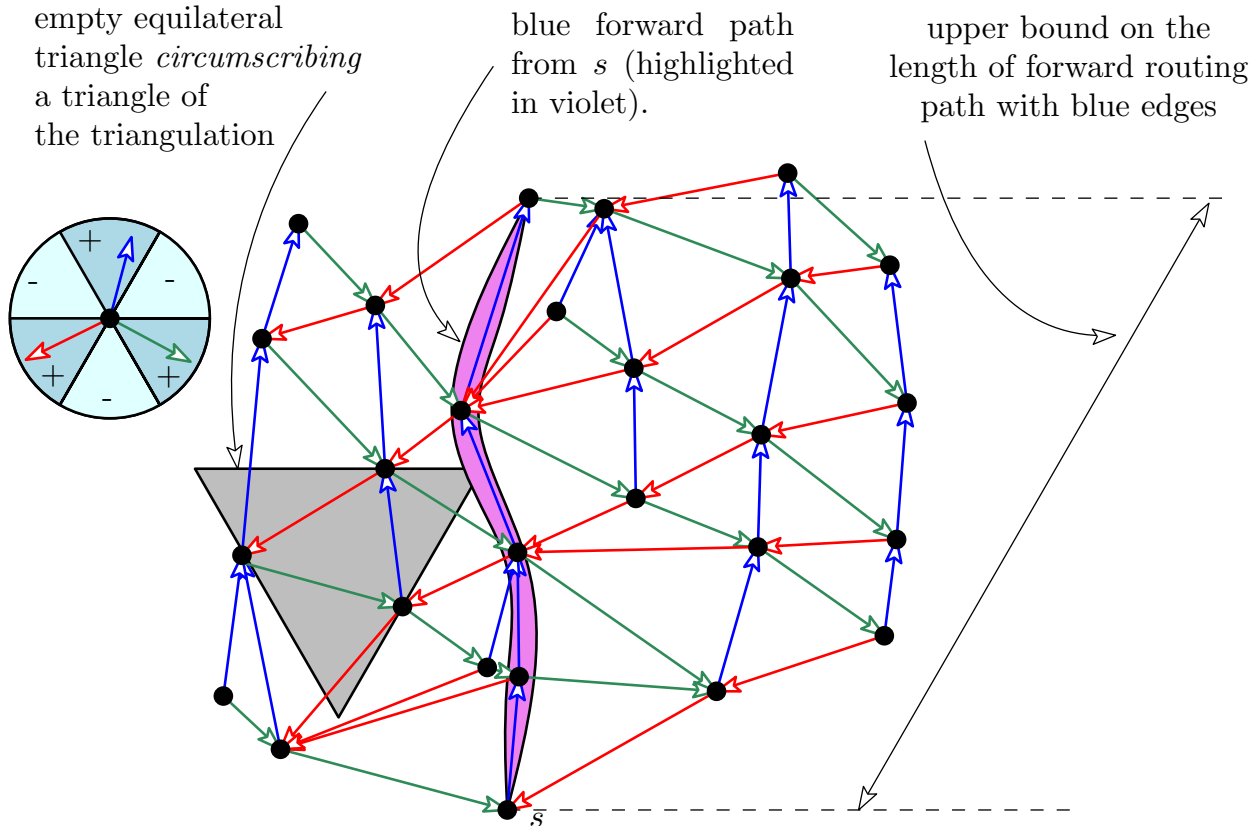


Figure 3: A  $TD$ -Delaunay triangulation (half- $\Theta_6$ -graph).

the one for the positive case are detailed in Sections 2.3 and 2.4. Since the worst-case optimal routing ratio is 2.89 and worst-case optimal spanning ratio is 2, this is one of the rare known separations between the spanning ratio and routing ratio of a spanner in the online setting [7]. In essence, even though there exists a path from  $s$  to  $t$  whose length is at most  $2\|st\|$ , no constant memory routing algorithm can find this path in the worst-case.

## 2 Two Basic Routing Building Blocks on the Half- $\Theta_6$ -graph

We introduce two routing modes on the half- $\Theta_6$ -graph which serve as building blocks for our routing algorithms that have optimal worst-case behaviour. We consider the even half- $\Theta_6$ -graph and for ease of reference, we color code the cones  $C_0, C_2$  and  $C_4$  blue, red, and green respectively. The two building blocks are: the *forward-routing phase* and the *side-routing phase*. Then these two building blocks are used to reformulate the routing algorithms proposed by Bose et al. [7].

### 2.1 Forward-Routing Phase

Forward-routing consists of only following edges defined by a specific type of cone (i.e., a cone with the same color) until some specified stopping condition is met. For example, suppose the specific cone selected for forward routing is the blue cone. Thus, when forward-routing is invoked at a vertex  $x$ , the edge followed is  $xy$  where  $y$  is the vertex adjacent to  $x$  in  $x$ 's blue cone. If the stopping condition is not met at  $y$ , then the

next edge followed is  $yz$  where  $z$  is the vertex adjacent to  $y$  in  $y$ 's blue cone. This process continues until a specified stopping condition is met. A path produced by forward routing consists of edges of the same color since edges are selected from one specific cone as illustrated in Figure 3.

**Lemma 1.** *Suppose that forward-routing is invoked at a vertex  $s$  and ends at a vertex  $t$ . The length of the path from  $s$  to  $t$  produced by forward-routing is at most the length of one side of the canonical triangle  $T_{st}$  which is  $\frac{2}{\sqrt{3}}$  times the length of the orthogonal projection of  $st$  onto the bisector of  $C_0^s$ .*

*Proof.* This result follows from the fact that each edge along the path makes a maximum angle of  $\frac{\pi}{6}$  with the cone bisector and the path is monotone in the direction of the cone bisector.  $\square$

## 2.2 Side-Routing Phase in the Half- $\Theta_6$ -graph

The *side-routing phase* is defined on the half- $\Theta_6$ -graph by using the fact that it is the *TD*-Delaunay triangulation, and thus planar. Consider a line  $\ell$  parallel to one of the cone sides. Without loss of generality, we will assume  $\ell$  is horizontal. We call the side of the line that bounds the even cones the *positive side* of  $\ell$ . For a horizontal line, the positive side is below  $\ell$ , and for the lines with slopes  $-\sqrt{3}$  and  $\sqrt{3}$ , respectively, the positive side is above the line. Let  $\Delta_1, \Delta_2, \Delta_3, \dots$  be an ordered sequence of consecutive triangles of the *TD*-Delaunay triangulation intersecting  $\ell$ . Let  $j \in \mathbb{N}^*$  and let  $B$  be the piece of the boundary of the union of the triangles  $\Delta_1, \dots, \Delta_j$  that goes from  $s$ , the bottom-left vertex of  $\Delta_1$ , to  $t$ , the bottom-right vertex of  $\Delta_j$ , below  $\ell$ . Note that  $B$  is a path in the half- $\Theta_6$ -graph. Side-routing invoked at vertex  $s$  along  $\ell$  stopping at  $t$  consists of walking from  $s$  to  $t$  along  $B$  (see Figure 4 for an example).

**Lemma 2.** *Side-routing on the positive side of a line  $\ell$  parallel to a cone boundary invoked at a vertex  $s$  and stopped at a vertex  $t$  in the half- $\Theta_6$ -graph results in a path whose length is bounded by twice the length of the orthogonal projection of  $st$  on  $\ell$ . This path only uses edges of two colors and all vertices of the path have their successor of the third color on the other side of  $\ell$ .*

*Proof.* Without loss of generality, assume  $\ell$  is horizontal and the positive side is below  $\ell$ . Consider the triangles  $\Delta_i, 1 \leq i \leq j$  as defined above. The empty equilateral triangle  $\nabla_i$  circumscribing  $\Delta_i$  has a vertex of  $\Delta_i$  on each of its sides by construction (the  $\nabla_i$  are shown in grey in Figure 4). If  $\Delta_i$  has an edge of the path (i.e., below  $\ell$ ) then the vertex on the horizontal side of  $\nabla_i$  is above the line while the two others are below. Thus, such an edge of the path goes from the left to the right side of  $\nabla_i$ . Based on the slopes of the edges of  $\nabla_i$ , we have the following:

- a– Each edge on the path has a length smaller than twice its horizontal projection. Therefore, summing the lengths of all the projections of the edges gives the claimed bound on the length.
- b– If the slope is negative, the path edge is green and if the slope is positive, the path edge is red.
- c– The blue successor of a vertex  $u$  of  $\Delta_i$  on the lower sides of  $\nabla_i$  is above  $\ell$  since the part of  $C_o^u$  below  $\ell$  is inside  $\nabla_i$  and thus contains no other points. Therefore, blue edges do not appear on the path.  $\square$

Notice that on the negative side of the line, we do not have the same properties. For example, the path above  $\ell$  in Figure 4 uses at least one edge of each color (the path above is highlighted in orange, note there is one blue edge circled in blue).

## 2.3 Positive in the Half- $\Theta_6$ -graph (and the $\Theta_6$ -graph)

If  $t$  is in a positive cone of  $s$ , Bose et al. [7] proposed a routing algorithm in the half- $\Theta_6$ -graph which they called *positive routing*. This algorithm consists of two phases: a *forward-routing* phase and a *side-routing* phase. The forward-routing phase is invoked with source  $s$  and destination  $t$ . It produces a path from  $s$  to the first vertex  $u$  outside the negative cone of  $t$  that contains  $s$ . The side-routing phase, invoked with source  $u$  and destination  $t$ , finds a path along the boundary of this negative cone.

For completeness, we give a proof of the following lemma shown in [7].

**Lemma 3.** *Positive routing has a worst-case routing ratio of 2.*

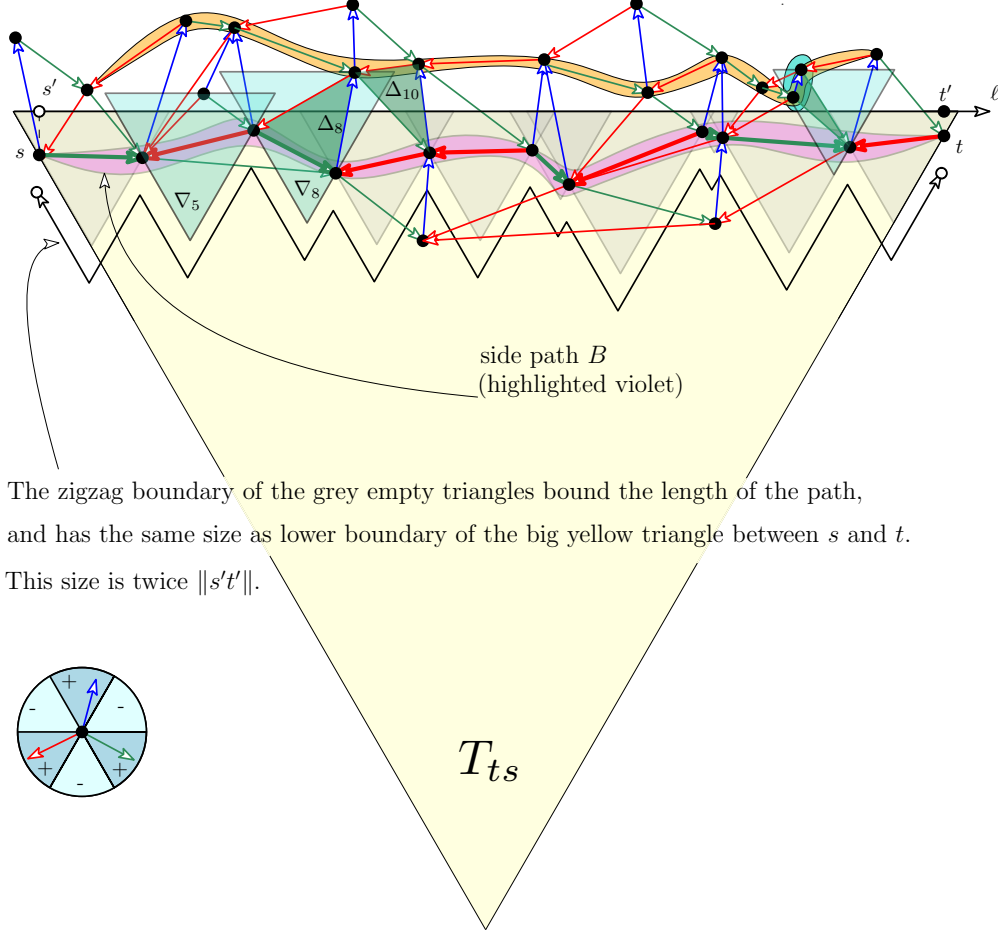


Figure 4: A side path below the horizontal line  $\ell$ .

*Proof.* Without loss of generality, we assume  $t$  is in the positive cone  $C_0^s$  and that the forward routing leaves the negative cone from  $t$  through its right side. Let  $u$  be the last vertex on the forward routing path,  $x, v$  the projections of  $u$  on  $\partial T_{st}$  (the boundary of  $T_{st}$ ) parallel to its sides;  $y$  the perpendicular projection of  $u$  on  $\partial T_{ts}$ ; and  $y'$  and  $y''$  horizontal projections of  $y$  on  $\partial T_{st}$  and line  $xu$  (see Figure 5-left). By Lemma 1, the length of the path from  $s$  to  $u$  is bounded by  $\|sv\| = \|sy'\| + \|y'v\|$  and by Lemma 2, the length of the path from  $u$  to  $t$  is bounded by  $2\|yt\| = \|xy''\| + (\|tx\| - \|y''y\|)$ . Since the triangle  $yy''u$  is isosceles we have  $\|yy''\| = \|y''u\| = \|y'v\| =: \beta$ . Combining the two paths, the total length is bounded by

$$\|sy'\| + \beta + \|y''x\| + \|tx\| - \beta = \|sy'\| + \|y'w\| + \|xt\| \leq \|sw\| + \|wt\|.$$

Thus, the stretch factor is smaller than  $\frac{\|sw\| + \|wt\|}{\|st\|}$ . Studying the function  $\xi \rightsquigarrow \frac{1+\xi}{\sqrt{\frac{3}{4} + (\xi - \frac{1}{2})^2}}$  and its derivative, this stretch factor is maximal and equal to 2 when  $\|wt\| = \|sw\|$  ( $\xi = \frac{\|wt\|}{\|sw\|} = 1$ )  $t$  in the upper left corner in Figure 5-left.  $\square$

## 2.4 Negative Routing in the Half- $\Theta_6$ -graph

When  $t$  is in a negative cone of  $s$ , Bose et al. [7] propose a routing strategy which they call *negative routing*. Without loss of generality, assume that  $t \in C_3^s$ , which implies that  $s \in C_0^t$  (i.e., the blue cone of  $t$  in Figure 5-

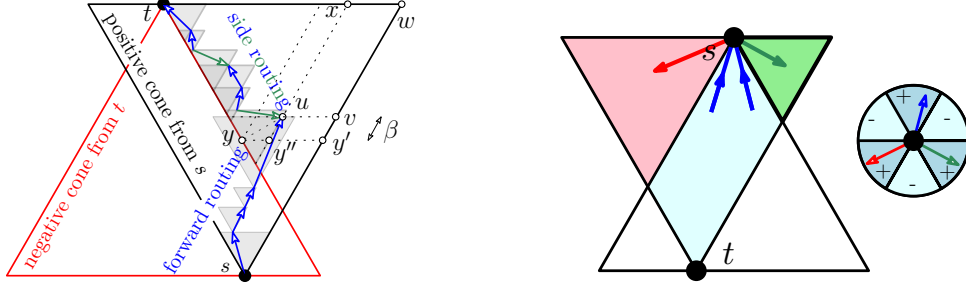


Figure 5: Positive and negative routing schemes [7].

right). Notice that  $T_{ts}$  is partitioned by  $T_{st}$  into three pieces, the portion contained in  $C_2^s$  (red cone of  $s$ ),  $C_3^s$  and  $C_4^s$  (green cone of  $s$ ). We refer to these three zones as: the red triangle, the blue region (which is the intersection of the blue cone of  $t$  with  $T_{st}$ ) and the green triangle. Without loss of generality, we assume that  $s$  is to the right of  $t$  and the green triangle is smaller than the red one.

Bose et al.'s algorithm [7] can be reformulated in the following way: If neither the green nor the red triangle is empty, negative routing follows the edge from  $s$  into the smaller of the two triangles. If one of the green or the red triangle is empty, negative routing uses one step of side routing along the side of the empty triangle (if both are empty, choose the larger of the two).

This process is iterated until  $t$  is reached. The worst-case stretch factor of this process is  $\frac{5}{\sqrt{3}} \simeq 2.89$  [7].

### 3 Alternative Negative Routing Algorithms in the Half- $\Theta_6$ -graph

In this section, we outline two alternatives to the negative routing algorithm described by Bose et al. [7]. Our algorithms are a little simpler to describe, have the same worst-case routing ratio, and are easier to analyze in the random setting. The lower bound of  $\frac{5}{\sqrt{3}} \simeq 2.89$  [7] applies to our alternative negative routing algorithms.

#### 3.1 Memoryless Routing

- Case 1. If  $t$  is in the positive cone  $C_i^s$  ( $i$  even), take one step of forward-routing in the direction of  $t$
- Case 2. If  $t$  is in the negative cone  $C_i^s$  ( $i$  odd) and the successor  $u$  of  $s$  in  $C_{i-1}^s$  is outside  $T_{ts}$  (red triangle empty), take one step of side-routing along the side of  $T_{ts}$  crossed by  $su$ .
- Case 3. If  $t$  is in the negative cone  $C_i^s$  ( $i$  odd) and the successor  $u$  of  $s$  in  $C_{i+1}^s$  is outside  $T_{ts}$  (green triangle empty), take one step of side-routing along the side of  $T_{ts}$  crossed by  $su$ .
- Case 4. If  $t$  is in the negative cone  $C_i^s$  ( $i$  odd) and both successors of  $s$  in  $C_{i-1}^s$  and  $C_{i+1}^s$  are inside  $T_{ts}$  (green and red triangle non empty), take one step of forward-routing in the direction of the side of  $T_{ts}$  incident to  $t$  closest to  $s$  (go to the green successor of  $s$ ).

Beyond the presentation, our strategy differs from the one of Bose et al. [7] in Case 4 where Bose et al. follows a blue edge if one exists.

We remark that when we reach Case 3, we enter a side-routing phase that will continue until  $t$  is reached since a side-routing step ensures that at the next iteration side-routing is still applicable.



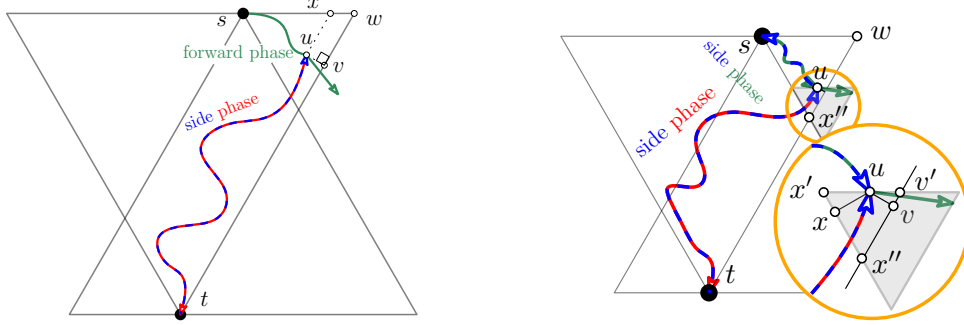


Figure 6: For Lemmas 4 and 5

The same argument holds in Case 2, unless we reach a point  $s$  with both successors outside  $T_{ts}$  in which case we follow the other side of  $T_{ts}$ .

To summarize, if  $t$  is in a positive cone of  $s$ , this routing algorithm will produce the path described in Section 2.3 and Lemma 3 applies. If  $t$  is in a negative cone of  $s$  we use a forward phase in the green triangle, until we reach a vertex  $u$  whose edge in the green triangle intersects  $T_{ts}$  (recall that we assume that the green triangle is the smaller one). At this point, we invoke side-routing from  $u$  to  $t$  along the boundary of  $T_{ts}$ .

**Lemma 4.** *Memoryless negative routing has a worst-case routing ratio of  $\frac{5}{\sqrt{3}} \simeq 2.89$ .*

*Proof.* Assume without loss of generality  $s \in C_0^t$ . Referring to Figure 6-left, let  $w$  be the upper right vertex of  $T_{ts}$ ,  $v$  be the orthogonal projection of  $u$  on  $tw$  and  $x$  its projection parallel to  $tw$  on  $sw$ . By Lemma 1, the path from  $s$  to  $u$  has length bounded by  $\|sx\|$  and by Lemma 2, the path from  $u$  to  $t$  has length bounded by  $2\|vt\|$ . Combining the two paths the length is bounded by  $\|sx\| + 2\|vt\| \leq \|sw\| + 2\|wt\|$ . Thus the stretch is smaller than  $\frac{\|sw\| + 2\|wt\|}{\|st\|}$ . Studying the function  $\xi \rightsquigarrow \frac{2+\xi}{\sqrt{\frac{3}{4} + (\xi - \frac{1}{2})^2}}$  this stretch factor attains its maximum value of  $\frac{5}{\sqrt{3}}$  when  $s$  and  $t$  lie on a vertical line ( $\xi = \frac{\|wt\|}{\|sw\|} = \frac{1}{2}$ ).  $\square$

### 3.2 Constant-Memory Negative Routing

We propose a second negative routing algorithm that has the same worst-case routing ratio, but we will prove that it has a better average routing ratio. However, it is no longer memoryless since it needs to remember the coordinates of one vertex, namely the source  $s$  of the path.

Let  $x''$  be the intersection between  $T_{ts}$  and  $T_{st}$  closest to  $s$ . (see Figure 6-right). The idea is to use side-routing from  $s$  along  $sx''$  and, just before exiting the green triangle, apply side-routing along  $x''t$ .

This routing algorithm is identical to the one in the previous subsection, except that we replace Case 4 with the following, where  $u$  is the current vertex and  $s$  is the origin of the path whose coordinates are kept in memory:

Case 4' If  $t$  is in the negative cone  $C_i^u$  ( $i$  odd) and both successors of  $u$  in  $C_{i-1}^u$  and  $C_{i+1}^u$  are inside  $T_{tu}$  (green and red triangle non empty): take one step of side-routing along the line  $sx''$ .

**Lemma 5.** *Constant-memory negative routing has a worst-case routing ratio of  $\frac{5}{\sqrt{3}} \simeq 2.89$ .*

*Proof.* Assume without loss of generality  $s \in C_0^t$ . Referring to the Figure 6-right, let  $x'$  and  $x$  be the horizontal and orthogonal projections of  $u$  on  $T_{st}$ , respectively, and  $v'$  and  $v$  be the horizontal and orthogonal projections of  $u$  on  $T_{ts}$ , respectively. By Lemma 2, the path from  $s$  to  $u$  has length bounded by  $2\|sx'\|$  and by Lemma 2 again, the path from  $u$  to  $t$  has length bounded by  $2\|vt\|$ . Combining the two paths the length is bounded by  $2\|sx'\| + 2\|vt\| \leq 2\|sx'\| + 2\|x'x\| + 2\|v't\| = 2\|wt\| + 2\|xx'\|$ . Since  $x$  is the orthogonal projection of  $u$  on

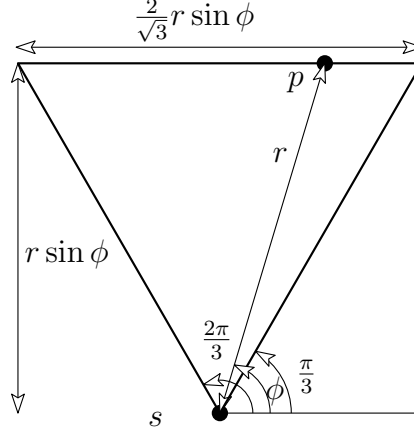


Figure 7: For Lemma 6.

the side  $x'x''$  of the equilateral triangle  $x'x''v'$ ,  $\|xx'\|$  is smaller than the half side of the triangle  $x'x''v'$  and we get a bound on the path length of  $2\|wt\| + 2\|xx'\| \leq 2\|wt\| + 2\frac{1}{2}\|x'v'\| \leq 2\|wt\| + \|sw\|$ . Therefore the result follows.  $\square$

## 4 Probabilistic Analysis

In this section, we develop tools to analyze the expected routing ratio of the routing algorithms defined in Sections 2 and 3 from a probabilistic point of view. In Section 4.1, we analyze the expected routing ratio of a forward-routing phase. In Section 4.2, we analyze the expected routing ratio of a side-routing phase. Then, using these results, we will analyze in Section 5 the expected routing ratio of four different routing algorithms.

### 4.1 Routing Ratio of a Forward-Routing Phase

Let  $X$  be a Poisson point process with intensity  $\lambda$  and consider the half- $\Theta_6$ -graph defined on  $X \cup \{s\}$ , where  $s$  is the origin. Let  $p_0 = s$  and  $p_{i+1}$  be the successor of  $p_i$  in the half- $\Theta_6$ -graph using the cone  $C_0^{p_i}$ . We define  $\tau_1 := \frac{\sqrt{3}}{12}(3 \ln 3 + 4)$ .

**Lemma 6.** *Let  $A > 0$  and  $\alpha = 2\sqrt{A}\lambda^{-\frac{1}{4}}\sqrt{\log(2A\sqrt{\lambda})}$ . Consider a forward-routing phase in the upward direction, starting at the origin until it crosses the line  $y = A$ . The expected routing ratio of this phase is  $\tau_1 + O\left(\frac{\alpha}{A}\right)$ . With probability greater than  $1 - \frac{17}{5}A^{-\frac{1}{2}}\lambda^{-\frac{1}{4}}$ , the endpoint of this phase lies in  $[-\alpha, \alpha] \times [A + 2\alpha]$ .*

*Proof.* Let  $p_0 = s, p_1, p_2, \dots, p_n$  denote the vertices of the forward path. We consider the following random variables:  $L_i$  is the Euclidean length of  $p_{i-1}p_i$ ,  $L_{x,i}$  is the signed length of the horizontal projection of  $p_{i-1}p_i$ , and  $L_{y,i}$  is the length of the vertical projection of  $p_{i-1}p_i$ .

Since  $C_0^{p_i}$  does not intersect  $T_{p_{i-1}p_i}$ , for different values of  $i$ , these variables are independent and identically distributed. Thus, when there is no ambiguity we denote them by  $L$ ,  $L_x$ , and  $L_y$ , respectively.

If  $p$  is the upward successor of  $s$  in the half- $\Theta_6$ -graph, then the upward triangle  $\mathcal{T}$  from  $s$  having  $p$  on its upper boundary is empty. Using polar coordinates where  $p = r(\cos \phi, \sin \phi)$ , the area of  $\mathcal{T}$ , denoted by  $\text{Area}(\mathcal{T})$ , is  $\frac{1}{\sqrt{3}}r^2 \sin^2 \phi$ . Thus  $\mathbb{P}[\mathcal{T} \text{ is empty}] = e^{-\lambda \text{Area}(\mathcal{T})} = e^{-\lambda \frac{1}{\sqrt{3}}r^2 \sin^2 \phi}$ , from which<sup>1</sup> (see Figure 7).

<sup>1</sup>Integral computations are available as a Maple worksheet with this paper on HAL repository.

$$\begin{aligned}
\mathbb{E}[L] = \mathbb{E}[L_1] &= \lambda \int_{p \in \text{BlueCone}} \mathbb{P}[p = p_1] \|p\| dp \\
&= \lambda \int_0^\infty \int_{\frac{\pi}{3}}^{\frac{2\pi}{3}} e^{-\lambda \frac{1}{\sqrt{3}} r^2 \sin^2 \phi} r^2 d\phi dr \\
&= \frac{1}{\sqrt{\lambda}} \frac{1}{2} 3^{-\frac{1}{4}} \sqrt{\pi} (1 + \frac{3}{4} \ln 3) \simeq \frac{1.228}{\sqrt{\lambda}}.
\end{aligned}$$

We define  $\mu := \frac{1}{2} 3^{-\frac{1}{4}} \sqrt{\pi} (1 + \frac{3}{4} \ln 3) \simeq 1.228$ . By symmetry, the expected length of the horizontal projection of an edge is  $\mathbb{E}[L_x] = 0$ . For the vertical projection, we get

$$\begin{aligned}
\mathbb{E}[L_y] &= \lambda \int_{p \in \text{BlueCone}} \mathbb{P}[p = p_1] y_p dp = \lambda \int_0^\infty \int_{\frac{\pi}{3}}^{\frac{2\pi}{3}} e^{-\lambda \frac{1}{\sqrt{3}} r^2 \sin^2 \phi} r^2 \sin \phi d\phi dr \\
&= \frac{1}{\sqrt{\lambda}} \frac{1}{2} 3^{\frac{1}{4}} \sqrt{\pi} \simeq \frac{1.166}{\sqrt{\lambda}}.
\end{aligned}$$

We define  $\mu_y := \frac{1}{2} 3^{\frac{1}{4}} \sqrt{\pi} \simeq 1.166$ . We prove that after  $n$  steps, the length of the path from  $p_0$  to  $p_n$  is approximately  $n \mathbb{E}[L] = \frac{n\mu}{\sqrt{\lambda}}$ , while the position of  $p_n$  is close to  $(n \mathbb{E}[L_x], n \mathbb{E}[L_y]) = (0, \frac{n\mu_y}{\sqrt{\lambda}})$ . This gives a routing ratio around  $\frac{\mu}{\mu_y}$ . Formally, let us first compute the higher order moments and define as follows the constants  $\sigma, \sigma_x, \sigma_y, \rho, \rho_x,$  and  $\rho_y$ .

$$\begin{aligned}
\mathbb{E}[L^2] &= \lambda \int_0^\infty \int_{\frac{\pi}{3}}^{\frac{2\pi}{3}} e^{-\lambda \frac{1}{\sqrt{3}} r^2 \sin^2 \phi} r^3 d\phi dr = \frac{10\sqrt{3}}{9\lambda} = \frac{\sigma^2}{\lambda}, \\
\mathbb{E}[L_x^2] &= \lambda \int_0^\infty \int_{\frac{\pi}{3}}^{\frac{2\pi}{3}} e^{-\lambda \frac{1}{\sqrt{3}} r^2 \sin^2 \phi} r^3 \cos^2 \phi d\phi dr = \frac{\sqrt{3}}{9\lambda} = \frac{\sigma_x^2}{\lambda}, \\
\mathbb{E}[L_y^2] &= \lambda \int_0^\infty \int_{\frac{\pi}{3}}^{\frac{2\pi}{3}} e^{-\lambda \frac{1}{\sqrt{3}} r^2 \sin^2 \phi} r^3 \sin^2 \phi d\phi dr = \frac{\sqrt{3}}{\lambda} = \frac{\sigma_y^2}{\lambda}, \\
\mathbb{E}[L^3] &= \lambda \int_0^\infty \int_{\frac{\pi}{3}}^{\frac{2\pi}{3}} e^{-\lambda \frac{1}{\sqrt{3}} r^2 \sin^2 \phi} r^4 d\phi dr = \frac{(27 \ln 3 + 68) \sqrt{\pi \sqrt{3}}}{64\lambda \sqrt{\lambda}} = \frac{\rho}{\lambda \sqrt{\lambda}}, \\
\mathbb{E}[|L_x|^3] &= 2\lambda \int_0^\infty \int_{\frac{\pi}{3}}^{\frac{\pi}{2}} e^{-\lambda \frac{1}{\sqrt{3}} r^2 \sin^2 \phi} r^4 \cos^3 \phi d\phi dr = \frac{3^{\frac{1}{4}} \sqrt{\pi}}{16\lambda \sqrt{\lambda}} = \frac{\rho_x}{\lambda \sqrt{\lambda}}, \\
\mathbb{E}[|L_y|^3] &= \lambda \int_0^\infty \int_{\frac{\pi}{3}}^{\frac{2\pi}{3}} e^{-\lambda \frac{1}{\sqrt{3}} r^2 \sin^2 \phi} r^4 \sin^3 \phi d\phi dr = \frac{3^{\frac{7}{4}} \sqrt{\pi}}{4\lambda \sqrt{\lambda}} = \frac{\rho_y}{\lambda \sqrt{\lambda}}.
\end{aligned}$$

For identically independently distributed variables  $X_i$ , each of which has expected value  $\mu_*$ , standard deviation  $\sigma_*$ , and third moment  $\rho_*$ , the *central limit theorem* states that

$$\mathbb{P} \left[ \left| \sum_{i=1}^n X_i - n\mu_* \right| \geq a\sigma_* \sqrt{n} \right] \rightsquigarrow \left( 1 - \operatorname{erf} \left( \frac{a}{\sqrt{2}} \right) \right),$$

when  $n$  tends to infinity, where  $\operatorname{erf}$  is the error function  $\operatorname{erf}(x) := \frac{1}{\sqrt{\pi}} \int_{-x}^x e^{-t^2} dt \in [-1, 1]$ . Then, the *Berry-Esseen inequality* specifies the rate of convergence:

$$\left| \mathbb{P} \left[ \left| \sum_{i=1}^n X_i - n\mu_* \right| \geq a\sigma_* \sqrt{n} \right] - \left( 1 - \operatorname{erf} \left( \frac{a}{\sqrt{2}} \right) \right) \right| \leq \frac{\rho_*}{2\sigma_*^3 \sqrt{n}}. \quad (1)$$

Applying Equation (1) to  $L_y$  with  $a = \sqrt{\log n}$  and using  $\operatorname{erf}(t) \geq 1 - \frac{e^{-t^2}}{\sqrt{\pi}t}$  for  $t \geq 0$ , we get

$$\begin{aligned}
\mathbb{P} \left[ \left| \sum_{i=1}^n L_{y,i} - n \frac{\mu_y}{\sqrt{\lambda}} \right| \geq \frac{\sigma_y}{\sqrt{\lambda}} \sqrt{n \log n} \right] &\leq \left( 1 - \operatorname{erf} \left( \sqrt{\frac{\log n}{2}} \right) \right) + \frac{\frac{\rho_y}{\lambda \sqrt{\lambda}}}{2 \left( \frac{\sigma_y}{\sqrt{\lambda}} \right)^3 \sqrt{n}} \\
&= \left( 1 - \operatorname{erf} \left( \sqrt{\frac{\log n}{2}} \right) \right) + \frac{\rho_y}{2\sigma_y^3 \sqrt{n}}. \\
&\leq \left( 1 - \left( 1 - \frac{\frac{1}{\sqrt{n}}}{\sqrt{\pi} \sqrt{\frac{\log n}{2}}} \right) \right) + \frac{\rho_y}{2\sigma_y^3 \sqrt{n}} \\
&= \frac{\sqrt{2}}{\sqrt{\pi} \sqrt{n \log n}} + \frac{\rho_y}{2\sigma_y^3 \sqrt{n}}.
\end{aligned}$$

Let  $n_A = \frac{(A+\alpha)\sqrt{\lambda}}{\mu_y}$ . For  $\lambda$  big enough we have  $\alpha = 2\sqrt{A}\lambda^{-\frac{1}{4}}\sqrt{\log(2A\sqrt{\lambda})}$  smaller than  $A$ , from which

$$\begin{aligned}
\frac{\sigma_y}{\sqrt{\lambda}} \sqrt{n_A \log n_A} &= \frac{\sigma_y}{\sqrt{\lambda}} \sqrt{\frac{(A+\alpha)\sqrt{\lambda}}{\mu_y} \log \frac{(A+\alpha)\sqrt{\lambda}}{\mu_y}} \\
&\leq \frac{\sigma_y}{\sqrt{\lambda}} \sqrt{\frac{2A\sqrt{\lambda}}{\mu_y} \log \frac{2A\sqrt{\lambda}}{\mu_y}} \\
&= \sigma_y \sqrt{\frac{2}{\mu_y} \sqrt{A}\lambda^{-\frac{1}{4}} \sqrt{\log\left(\frac{2}{\mu_y} A\sqrt{\lambda}\right)}} \\
&\leq 3^{\frac{1}{4}} \sqrt{\frac{2}{\frac{1}{2} 3^{\frac{1}{4}} \sqrt{\pi}}} \sqrt{A}\lambda^{-\frac{1}{4}} \sqrt{\log(2A\sqrt{\lambda})} \\
&\leq 1.73 \sqrt{A}\lambda^{-\frac{1}{4}} \sqrt{\log(2A\sqrt{\lambda})} \\
&\leq 2\sqrt{A}\lambda^{-\frac{1}{4}} \sqrt{\log(2A\sqrt{\lambda})} = \alpha.
\end{aligned}$$

$$\begin{aligned}
\mathbb{P} \left[ \left| \sum_{i=1}^{n_A} L_{y,i} - A - \alpha \right| \geq \alpha \right] &\leq \mathbb{P} \left[ \left| \sum_{i=1}^{n_A} L_{y,i} - A - \alpha \right| \geq \frac{\sigma_y}{\sqrt{\lambda}} \sqrt{n_A \log n_A} \right] \\
&\leq \frac{\sqrt{2}}{\sqrt{\pi} \sqrt{n_A \log n_A}} + \frac{\rho_y}{2\sigma_y^3 \sqrt{n_A}} \\
&\leq \frac{1}{\sqrt{n_A}} \left( \sqrt{\frac{2}{\pi}} + \frac{\rho_y}{2\sigma_y^3} \right) \\
&\leq \sqrt{\frac{\mu_y}{A\sqrt{\lambda}}} \left( \sqrt{\frac{2}{\pi}} + \frac{\rho_y}{2\sigma_y^3} \right).
\end{aligned}$$

Now we look at the  $x$ -coordinate of  $p_{n_A}$ , which is  $\sum_{i=1}^{n_A} L_{x,i}$ . Using Equation (1) again, we have

$$\mathbb{P} \left[ \left| \sum_{i=1}^{n_A} L_{x,i} \right| \geq \frac{\sigma_x}{\sqrt{\lambda}} \sqrt{n_A \log n_A} \right] \leq \left( 1 - \operatorname{erf} \left( \sqrt{\frac{\log n_A}{2}} \right) \right) + \frac{\rho_x}{2\sigma_x^3 \sqrt{n_A}}.$$

Substituting for  $n_A$  and since  $\alpha \geq \frac{\sigma_x}{\sqrt{\lambda}} \sqrt{n_A \log n_A}$  (for  $\lambda$  big enough), we get

$$\mathbb{P} \left[ \left| \sum_{i=1}^{n_A} L_{x,i} \right| \geq \alpha \right] \leq \sqrt{\frac{\mu_y}{A\sqrt{\lambda}}} \left( \sqrt{\frac{2}{\pi}} + \frac{\rho_x}{2\sigma_x^3} \right).$$

Thus,

$$\begin{aligned}
\mathbb{P}[p_{n_A} \in [-\alpha, \alpha] \times [A, A + 2\alpha]] &\leq \sqrt{\frac{\mu_y}{A\sqrt{\lambda}}} \left( 2\sqrt{\frac{2}{\pi}} + \frac{\rho_x}{2\sigma_x^3} + \frac{\rho_y}{2\sigma_y^3} \right) \\
&= \sqrt{\frac{1}{2} 3^{\frac{1}{4}} \sqrt{\pi}} \left( 2\sqrt{\frac{2}{\pi}} + \frac{3^{\frac{1}{4}} \sqrt{\pi}}{16} + \frac{3^{\frac{7}{4}} \sqrt{\pi}}{2(3^{\frac{1}{4}})^3} \right) A^{-\frac{1}{2}} \lambda^{-\frac{1}{4}} \\
&\leq 3.4 A^{-\frac{1}{2}} \lambda^{-\frac{1}{4}}.
\end{aligned}$$

Let  $i_A$  be the smallest  $i$  such that  $y_{p_i} \geq A$ . If  $i_A \leq n_A$ , then  $y_{p_{n_A}} \geq y_{p_{i_A}} \geq A$ . We can bound  $\|p_0 p_{i_A}\| > A$  and the path length  $\sum_{i=1}^{i_A} L_i \leq \sum_{i=1}^{n_A} L_i \leq n_A \mathbb{E}[L]$ . If  $i_A > n_A$ , we can bound the routing ratio by  $\frac{2}{\sqrt{3}}$  using Lemma 1 (worst-case analysis of forward-routing).

$$\begin{aligned}
\mathbb{E} \left[ \frac{\sum_{i=1}^{i_A} L_i}{\|p_0 p_{i_A}\|} \right] &\leq \mathbb{P}[i_A \leq n_A] \mathbb{E} \left[ \frac{\sum_{i=1}^{i_A} L_i}{\|p_0 p_{i_A}\|} \right] + \mathbb{P}[i_A > n_A] \frac{2}{\sqrt{3}} \\
&\leq 1 \cdot \frac{n_A \cdot \mathbb{E}[L]}{A} + \sqrt{\frac{\mu_y}{A\sqrt{\lambda}}} \left( \sqrt{\frac{2}{\pi}} + \frac{\rho_y}{2\sigma_y^3} \right) \frac{2}{\sqrt{3}} \\
&\leq \frac{(A+\alpha)\sqrt{\lambda} \frac{\mu}{\sqrt{\lambda}}}{A} + \sqrt{\frac{4\mu_y}{3}} \left( \sqrt{\frac{2}{\pi}} + \frac{\rho_y}{2\sigma_y^3} \right) \frac{1}{A\sqrt{\lambda}} \\
&= \frac{\mu}{\mu_y} + O \left( A^{-\frac{1}{2}} \lambda^{-\frac{1}{4}} \sqrt{\log(2A\sqrt{\lambda})} \right) + O \left( \frac{1}{A\sqrt{\lambda}} \right) \\
&= \frac{\sqrt{3}}{12} (3 \ln 3 + 4) + O \left( A^{-\frac{1}{2}} \lambda^{-\frac{1}{4}} \sqrt{\log(2A\sqrt{\lambda})} \right). \quad \square
\end{aligned}$$

**Remark 7.**  $\Theta_6$ -routing in a dense point set runs in two phases, while the target is really inside a cone, it has a similar behavior to forward-routing. When it reaches the boundary of a cone, it switches between two cones (one odd and one even) and a similar analysis can be done. However, measuring the progress along the cone boundary instead of the cone bisector gives an expected routing ratio of  $\tau_2 := \frac{2}{\sqrt{3}} \tau_1 = \frac{1}{6} (3 \ln 3 + 4)$ .

## 4.2 Routing Ratio of a Side-Routing Phase

To analyze the expected routing ratio of a side-routing phase, we consider the sum of the lengths of all of its edges. Then, we use the *Slivnyak-Mecke formula* (refer to [17, Corollary 3.2.3]) to transform this sum into an integral, from which we get the following lemma.

**Lemma 8.** Consider a side-routing phase in the horizontal direction, starting at the origin until it reaches the line  $x = A$ . The expected routing ratio of this phase is  $\tau_2 + O(A^{-1} \lambda^{-\frac{1}{2}})$  with  $\tau_2 := \frac{2}{\sqrt{3}} \tau_1$ .

*Proof.* Up to a scaling factor of  $A$  on the lengths and  $A^2$  on the density, we can assume without loss of generality that  $A = 1$ . Let  $\nabla(p, q)$  denote the equilateral triangle with  $p$  on its left side,  $q$  on its right side and its horizontal side supported by the  $x$ -axis (the triangle is below the  $x$ -axis). Let  $s = (0, 0)$  and  $t = (1, 0)$ . The following analysis sums up the lengths of the edges  $pq$  of the half- $\Theta_6$ -graph of  $X$ , where  $p, q \in \nabla(s, t)$  and  $\nabla(p, q)$  is empty. Depending on the situation, we may have to add an edge that connects the path to  $s$  and/or to  $t$  if these points have been added to the point set. We may also have to add an edge that crosses the boundary of  $\nabla(s, t)$ . In any case, the expected length of these edges is  $O\left(\frac{1}{\sqrt{\lambda}}\right)$ , which is negligible. Using Slivnyak-Mecke formula, we have

$$\mathbb{E}[\text{length}] = \mathbb{E} \left[ \sum_{p, q \in X \cap \nabla(s, t)} \mathbb{1}_{[\nabla(p, q) \cap X = \emptyset]} \|pq\| \right] = \lambda^2 \iint_{p, q \in \nabla(s, t)} e^{\lambda \text{Area}(\nabla(p, q))} \|pq\| dq dp.$$

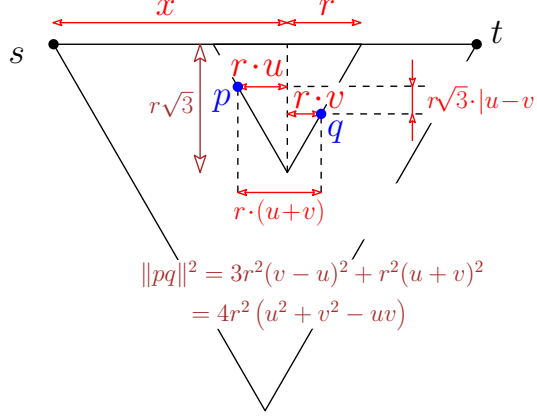


Figure 8: For Lemma 8.

To solve this integral, we first define  $\Phi$  the following variable substitution (see Figure 8).

$$\begin{aligned} \Phi : \mathbb{R} \times \mathbb{R}_{\geq 0} \times [0, 1]^2 &\rightarrow (\mathbb{R}^2)^2 \\ (x, r, u, v) &\rightsquigarrow \left( \begin{pmatrix} x - ru \\ -\sqrt{3}r(1-u) \end{pmatrix}, \begin{pmatrix} x + rv \\ -\sqrt{3}r(1-v) \end{pmatrix} \right). \end{aligned}$$

The Jacobian of  $\Phi$  is

$$\det(J_{\Phi}) = \begin{vmatrix} 1 & -u & -r & 0 \\ 0 & -\sqrt{3}(1-u) & \sqrt{3}r & 0 \\ 1 & v & 0 & r \\ 0 & -\sqrt{3}(1-v) & 0 & \sqrt{3}r \end{vmatrix} = -6r^2.$$

This variable substitution yields

$$\begin{aligned} \mathbb{E}[\text{length}] &= \lambda^2 \int_0^1 \int_0^{\min(x, 1-x)} \int_0^1 \int_0^1 e^{-\lambda r^2 \sqrt{3}} r 2\sqrt{u^2 + v^2 - uv} \cdot |\det(J_{\Phi})| \, dv du dr dx \\ &= \lambda^2 \left( \int_0^1 \int_0^{\min(x, 1-x)} e^{-\lambda r^2 \sqrt{3}} r \cdot 6 \cdot r^2 dr dx \right) \left( 2 \int_0^1 \int_0^1 \sqrt{u^2 + v^2 - uv} \, dv du \right) \\ &= \lambda^2 \left( 2 \cdot \int_0^{\frac{1}{2}} \int_0^x 6e^{-\lambda r^2 \sqrt{3}} \cdot r^3 dr dx \right) \left( 4 \int_0^1 \int_0^u \sqrt{u^2 + v^2 - uv} \, dv du \right) \\ &= 8\lambda^2 \cdot \frac{1}{4\lambda^2} \left( 2 + 3^{\frac{3}{4}} \sqrt{\pi} \operatorname{erf} \left( \frac{1}{2} \sqrt{\lambda} \sqrt[4]{3} \right) \frac{1}{\sqrt{\lambda}} + e^{-\frac{1}{4} \lambda \sqrt{3}} \right) \left( \frac{1}{6} + \frac{\ln 3}{8} \right) \\ &= \frac{1}{6} (3 \ln 3 + 4) + O\left(\frac{1}{\sqrt{\lambda}}\right) = \tau_2 + O\left(\frac{1}{\sqrt{\lambda}}\right) \simeq 1.2160 + O\left(\frac{1}{\sqrt{\lambda}}\right). \quad \square \end{aligned}$$

Observe that side-routing and  $\Theta_6$ -routing in the neighbourhood of a cone boundary have the same expected routing ratio. This means that in side-routing, the expected progress made by an edge of the path behaves as if it was independent from the previous edges, although this is not the case a priori.

## 5 Wrap Up

In this section, we analyze the routing algorithms defined in Sections 2 and 3 using the tools from Section 4. Recall that these algorithms are made of two phases. The analysis is based on the following two ingredients. First, the splitting point between the two phases belongs to a small region of the plane with high probability. Second, the two phases of each routing algorithm can be analyzed separately.

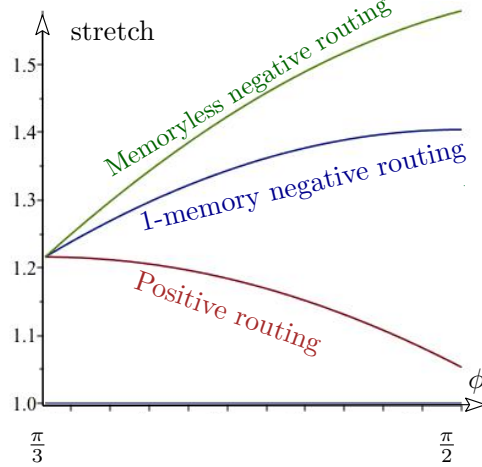


Figure 9: Theorem 9.

**Theorem 9.** Let  $X$  be a Poisson point process with intensity  $\lambda$ . Consider the positive and the two alternative negative routing algorithms on the half- $\Theta_6$ -graph defined on  $X \cup \{s, t\}$ , where  $s$  and  $t$  are two points at unit distance. Figure 9 presents a graph of the expected routing ratios of the different routing algorithms as  $\lambda$  tends to  $\infty$  in terms of  $\phi$  the angle of  $st$  with the horizontal axis. The following table shows the expected stretch for a given  $\phi$  and also the maximum for all  $\phi$  and average on  $\phi$ .

Routing	$\mathbb{E}[\text{routing ratio}](\phi)$	$\max_{s,t} \mathbb{E}[\text{routing ratio}]$	$\mathbb{E}_{s,t}[\mathbb{E}[\text{routing ratio}]]$
Positive routing	$\tau_1 \left( \sin \phi + \frac{1}{\sqrt{3}} \cos \phi \right)$	$\frac{2}{\sqrt{3}} \tau_1 \simeq 1.2160$	$\frac{2\sqrt{3}}{\pi} \tau_1 \simeq 1.1612$
Constant-memory	$\frac{4}{3} \tau_1 \sin \phi$	$\frac{4}{3} \tau_1 \simeq 1.4041$	$\frac{4}{\pi} \tau_1 \simeq 1.3408$
Memoryless	$\tau_1 \left( \frac{3}{2} \sin \phi - \frac{\sqrt{3}}{6} \cos \phi \right)$	$\frac{3}{2} \tau_1 \simeq 1.5800$	$\frac{6-\sqrt{3}}{\pi} \tau_1 \simeq 1.4306$

$$\tau_1 := \frac{1}{4\sqrt{3}}(3 \ln 3 + 4)$$

*Proof.* Each of the four routing algorithms we consider is the combination of two phases, each of which can be a forward-routing phase or a side-routing phase. These two phases articulate at a splitting point  $w \in X$ , where the routing algorithm changes from one phase to the next. The actual splitting point is close to an *ideal splitting point*  $w_*$  (which does not belong to  $X$ ) that depends only on  $s, t$  and the routing algorithm. Therefore, the analysis of each of the four routing algorithms follows the same scheme: let the expected routing ratio of the two phases be  $\tau$  and  $\tau'$ , respectively. Since the point  $w$  is close to  $w_*$  with high probability, the expected routing ratio of the routing algorithm is  $\frac{\|sw_*\|\tau + \|w_*t\|\tau'}{\|st\|}$  (see Figure 10-left).

Positive routing is made of a forward-routing phase from  $s$  to  $w$  followed by a side phase from  $w$  to  $t$  (see Section 2.3). If we fix  $s = (0, 0)$  and  $t = (\cos \phi, \sin \phi)$  for  $\phi \in [\frac{\pi}{3}, \frac{\pi}{2}]$ , the splitting point becomes  $w_+ = (0, 1 - \sqrt{3} \sin \phi)$ . With probability less than  $4\lambda^{-\frac{1}{4}}$  we bound the routing ratio by the worst case bounds, i.e., between 1 and 2. Otherwise, we use the fact that the splitting point  $w$  is close to  $w_+$ . Let  $A = 1 - \sqrt{3} \cos \phi$  and  $\alpha = 2\sqrt{A}\lambda^{-\frac{1}{4}}\sqrt{\log(2A\sqrt{\lambda})}$ . We have  $\|w_+w\| < 3\alpha$  with probability greater than  $1 - 4\lambda^{-\frac{1}{4}}$ , by Lemma 6. Moreover, by Lemmas 6 and 8,  $\tau = \tau_1$  and  $\tau' = \tau_2$ . Thus, the expected routing ratio  $\psi := \mathbb{E} \left[ \frac{\tau_1 \|sw\| + \tau_2 \|wt\|}{\|st\|} \right]$  satisfies

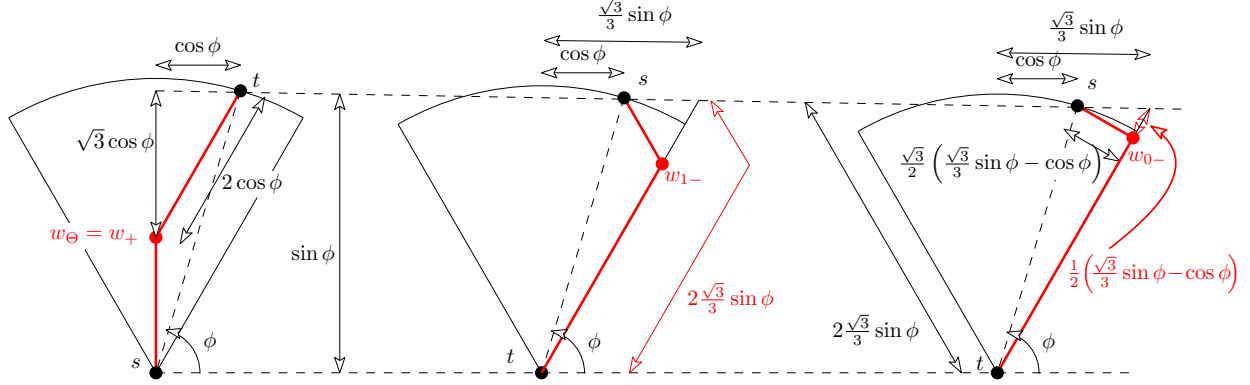


Figure 10: For the proof of Theorem 9.

$$\begin{aligned}
\psi &\leq \mathbb{P}[\|w_+w\| \geq \alpha] 2 + (1 - \mathbb{P}[\|w_+w\| \geq \alpha]) \left( \frac{\tau_1 \|sw_+\| + \tau_2 \|w_+t\|}{\|st\|} + \frac{(\tau_1 + \tau_2) \|ww_+\|}{\|st\|} \right) \\
\psi &\geq \mathbb{P}[\|w_+w\| \geq \alpha] 1 + (1 - \mathbb{P}[\|w_+w\| \geq \alpha]) \left( \frac{\tau_1 \|sw_+\| + \tau_2 \|w_+t\|}{\|st\|} - \frac{(\tau_1 + \tau_2) \|ww_+\|}{\|st\|} \right) \\
\psi &= \frac{\tau_1 \|sw_+\| + \tau_2 \|w_+t\|}{\|st\|} + O(\lambda^{-\frac{1}{4}} \sqrt{\log \lambda})
\end{aligned}$$

And we get as a limit when  $\lambda \rightarrow \infty$ :

$$\frac{\tau_1 \|sw_+\| + \tau_2 \|w_+t\|}{\|st\|} = \tau_1 (\sin \phi - \sqrt{3} \cos \phi) + \tau_2 2 \cos \phi = \tau_1 \left( \sin \phi + \frac{1}{\sqrt{3}} \cos \phi \right),$$

whose maximum value is  $\frac{2}{\sqrt{3}}\tau_1 \simeq 1.2160$ , obtained for  $\phi = \frac{\pi}{3}$ . Considering any direction equally likely, average on  $\phi$  to get an expected value of

$$\frac{6}{\pi} \int_{\frac{\pi}{3}}^{\frac{\pi}{2}} \tau_1 \left( \sin \phi + \frac{1}{\sqrt{3}} \cos \phi \right) d\phi = \frac{2\sqrt{3}}{\pi} \tau_1 \simeq 1.1612.$$

**Remark 10.** By Remark 7, a similar analysis can be done for  $\Theta_6$ -routing with the same splitting point, giving the same expected ratio as with positive routing.

Constant-memory routing is made of a side-routing phase from  $s$  to  $w$ , followed by a side-routing phase from  $w$  to  $t$  (see Section 3.2). If we fix  $t = (0, 0)$  and  $s = (\cos \phi, \sin \phi)$  for  $\phi \in [\frac{\pi}{3}, \frac{\pi}{2}]$ , the splitting point becomes  $w_{1-} = \left( \frac{\sqrt{3}}{3} \sin \phi - \cos \phi \right) \left( 1, \frac{\sqrt{3}}{3} \right)$ . By Lemma 8,  $\|w_{1-}w\| < O(\lambda^{-\frac{1}{2}})$  with high probability. Moreover, by Lemma 8,  $\tau = \tau' = \tau_2$ . Thus, the expected routing ratio when  $\lambda \rightarrow \infty$  is (see Figure 10-center).

$$\tau_2 \frac{\|sw_{1-}\| + \|w_{1-}t\|}{\|st\|} = \tau_2 2 \frac{\sqrt{3}}{3} \sin \phi = \frac{4}{3} \tau_1 \sin \phi,$$

whose maximum is  $\frac{4}{3}\tau_1 \simeq 1.4041$ , obtained for  $\phi = \frac{\pi}{2}$ . Averaging on  $\phi$  yields an expected value of

$$\frac{6}{\pi} \int_{\frac{\pi}{3}}^{\frac{\pi}{2}} \frac{4}{3} \tau_1 \sin \phi d\phi = \frac{4}{\pi} \tau_1 \simeq 1.3408.$$



Memoryless negative routing is made of a forward-routing phase from  $s$  to  $w$ , followed by a side phase from  $w$  to  $t$  (see Section 3.1). If we fix  $t = (0, 0)$  and  $s = (\cos \phi, \sin \phi)$  for  $\phi \in [\frac{\pi}{3}, \frac{\pi}{2}]$ , the splitting point becomes  $w_{0-}$  the orthogonal projection of  $s$  on the side of  $T_{ts}$  (see Figure 10-right). By Lemma 6,  $\|w_{0-} - w\| < O(\lambda^{-\frac{1}{4}} \sqrt{\log \lambda})$  with probability greater than  $1 - O(\lambda^{-\frac{1}{4}})$ . Moreover, by Lemmas 6 and 8,  $\tau = \tau_1$  and  $\tau' = \tau_2$ . Thus, the limit of the expected routing ratio is

$$\begin{aligned} \frac{\tau_1 \|sw_{0-}\| + \tau_2 \|w_{0-}t\|}{\|st\|} &= \tau_1 \left( \frac{\sqrt{3}}{2} \left( \frac{\sqrt{3}}{3} \sin \phi - \cos \phi \right) \right) + \tau_2 \left( 2 \frac{\sqrt{3}}{3} \sin \phi - \frac{1}{2} \left( \frac{\sqrt{3}}{3} \sin \phi - \cos \phi \right) \right) \\ &= \tau_1 \left( \frac{3}{2} \sin \phi - \frac{\sqrt{3}}{6} \cos \phi \right), \end{aligned}$$

whose maximum is  $\frac{3}{2}\tau_1 \simeq 1.5800$ , obtained for  $\phi = \frac{\pi}{2}$ . Averaging on  $\phi$  yields an expected value of

$$\frac{6}{\pi} \int_{\frac{\pi}{3}}^{\frac{\pi}{2}} \tau_1 \left( \frac{3}{2} \sin \phi - \frac{\sqrt{3}}{6} \cos \phi \right) d\phi = \frac{6-\sqrt{3}}{\pi} \tau_1 \simeq 1.4306.$$

Figure 9 depicts the expected routing ratios as functions of  $\phi$ . □

## Acknowledgements

The authors would like to thank Nicolas Chenavier for interesting discussions related to this paper.

## References

- [1] Oswin Aichholzer, Sang Won Bae, Luis Barba, Prosenjit Bose, Matias Korman, André van Renssen, Perouz Taslakian, and Sander Verdonschot. Theta-3 is connected. *Computational Geometry: Theory and Applications*, 47(9):910–917, 2014.
- [2] Nicolas Bonichon, Cyril Gavoille, Nicolas Hanusse, and David Ilcinkas. Connections between Theta-graphs, Delaunay triangulations, and orthogonal surfaces. In *Proceedings of the 36th International Conference on Graph Theoretic Concepts in Computer Science (WG 2010)*, pages 266–278, 2010.
- [3] Nicolas Bonichon and Jean-François Marckert. Asymptotics of geometrical navigation on a random set of points in the plane. *Advances in Applied Probability*, 43(4):899–942, 2011. doi:10.1239/aap/1324045692.
- [4] P. Bose and P. Morin. Online routing in triangulations. *SIAM Journal on Computing*, 33(4):937–951, 2004.
- [5] Prosenjit Bose, Jean-Lou De Carufel, Darryl Hill, and Michiel H. M. Smid. On the spanning and routing ratio of theta-four. In *SODA*, pages 2361–2370. SIAM, 2019.
- [6] Prosenjit Bose, Jean-Lou De Carufel, Pat Morin, André van Renssen, and Sander Verdonschot. Towards tight bounds on theta-graphs: More is not always better. *Theoretical Computer Science*, 616:70–93, 2016.
- [7] Prosenjit Bose, Rolf Fagerberg, André van Renssen, and Sander Verdonschot. Optimal local routing on Delaunay triangulations defined by empty equilateral triangles. *SIAM Journal on Computing*, 44(6):1626–1649, 2015. doi:10.1137/140988103.
- [8] Prosenjit Bose, Pat Morin, André van Renssen, and Sander Verdonschot. The  $\Theta_5$ -graph is a spanner. *Computational Geometry: Theory and Applications*, 48(2):108 – 119, 2015. doi:10.1016/j.comgeo.2014.08.005.
- [9] Prosenjit Bose and Michiel Smid. On plane geometric spanners: A survey and open problems. *Computational Geometry: Theory and Applications*, 46(7):818–830, 2013.

- [10] Paul Chew. There are planar graphs almost as good as the complete graph. *Journal of Computer and System Sciences*, 39(2):205–219, 1989.
- [11] E. W. Dijkstra. A note on two problems in connexion with graphs. *Numerische Mathematik*, 1:269–271, 1959.
- [12] J. E. Hopcroft and R. E. Tarjan. Algorithm 447: Efficient algorithms for graph manipulation. *Communications of the ACM*, 16(6):372–378, 1973.
- [13] C. Y. Lee. An algorithm for path connection and its applications. *IRE Transaction on Electronic Computers*, EC-10(3):346–365, 1961.
- [14] E. F. Moore. The shortest path through a maze. In *Proceedings of the International Symposium on the Theory of Switching*, pages 285–292, 1959.
- [15] G. Narasimhan and M. Smid. *Geometric Spanner Networks*. Cambridge University Press, 2007.
- [16] Jim Ruppert and Raimund Seidel. Approximating the d-dimensional complete euclidean graph. In *Proceedings of the 3rd Canadian Conference on Computational Geometry (CCCG 1991)*, pages 207–210, 1991.
- [17] R. Schneider and W. Weil. *Stochastic and Integral Geometry*. Probability and Its Applications. Springer Berlin Heidelberg, 2008.